Design of a Test Apparatus to Study a Proposed Dynamic Tissue Puncture Model

by

Kathleen Marie Inman

Submitted to the
Department of Mechanical Engineering
in Partial Fulfillment of the Requirements for the Degree of

Bachelor of Science

at the

Massachusetts Institute of Technology

June 2013

© 2013 Inman
All Rights Reserved
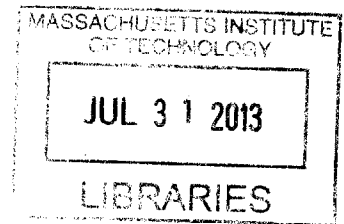
The author hereby grants to MIT permission to reproduce and to distribute publicly
paper and electronic copies of this thesis document in whole or in part in any medium
now known or hereafter created.

Signature of Author...
Department of Mechanical Engineering
May 15, 2013

Certified by ....
Alexander Slocum
Neil and Jane Pappalardo Professor of Mechanical Engineering
MacVicar Faculty Fellow
Thesis Supervisor

Accepted by...
Accepted by: Annette Hosoi
Associate Professor of Mechanical Engineering
Undergraduate Officer

Design of a Test Apparatus to Study a Proposed Dynamic Tissue Puncture Model

by

Kathleen M. Inman

Submitted to the Department of Mechanical Engineering
on May 15, 2013 in partial fulfillment of the
requirements for the degree of Bachelor of Science in
Mechanical Engineering

Abstract

Two test apparatuses were designed, built, and evaluated in order to study a proposed dynamic tissue puncture model. The test apparatuses were designed to improve existing experiments used previously to experimentally verify tissue models. These models are incomplete due to the small range of velocities tested (up to 250 mm/s) and because they do not account for the complex interactions between tissue and needle during deep puncture. The first test apparatus is based on a vertical drop test. This apparatus was modeled, built, and evaluated for its performance based on the speeds achieved in the region of impact. Based on improvements from this apparatus, a second test apparatus was modeled and will be built in the future. The second apparatus is a modified drop test; however, it is on an inclined plane in order to reduce the effects of gravity when attempting to achieve lower speeds.

Thesis Supervisor: Alexander H. Slocum

Title: Neil and Jane Pappalardo Professor of Mechanical Engineering, MacVicar Faculty Fellow

Acknowledgments

Table of Contents

List of Figures

List of Tables

1. Introduction

1.1 Soft Tissue Puncture Access

1.1.1 Description of Procedures

Soft tissue puncture access is an element of a variety of medical procedures including IV placement, epidurals, cardiac catheter insertion, and laparoscopic surgery. It generally involves the use of a cannula (such as a trocar or epidural) and needle system. Figure 1 shows an example of such a system.
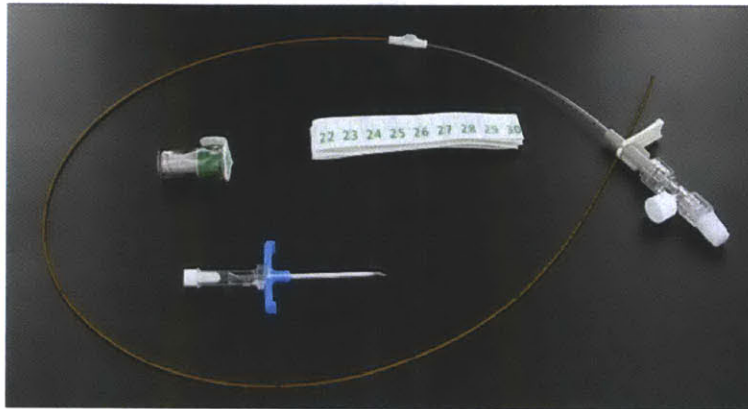
Figure 1: A flexible catheter system. The catheter is placed in a vein and a needle threaded through the brown tubing to acquire a sample at the other end.

The needle-cannula system is used to gain access and the cannula is left behind as a pathway into the body. During procedures that involve the use of a needle and cannula the tissue involved is inhomogeneous and compliant making it difficult to achieve precise punctures. Precision is very important, for example, in the case of tumor sampling. If a sample is taken of tissue near to but not including the tumor a false negative result occurs which could be potentially life threatening.

1.1.2 Current Issues

As mentioned before, there are many difficulties and dangers in taking samples and manipulating tissue deep within the body. It is for this reason that scientists have attempted to develop dynamic models for tissue to better describe their behavior. Figure 2 depicts one such model:
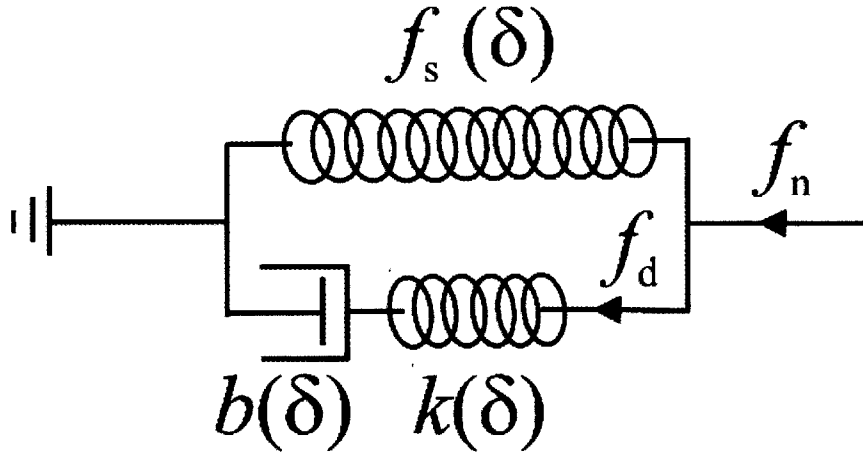
Figure 2: The modified Kelvin model used to describe the viscoelastic nature of tissue. [3]

Where $b(\delta)$ is the nonlinear deflection-dependent damping coefficient for the dashpot, f_n is the needle force, $k(\delta)$ is the deflection-dependent nonlinear spring constant, $f_s(\delta)$ is a nonlinear force-deformation function to describe the static component of the needle force, and f_d is the nonlinear force-deformation function to describe the dynamic part of the model.

These models have been employed to study puncture access and estimate optimum speed, angle, needle shape, etc. to decrease the effects of deflection and interaction between the needle and the tissue. However, recent experiments suggest that this model may be incomplete and requires more careful examination. A more complete tissue model is currently being theoretically determined and computationally modeled. It is necessary to experimentally verify these results. Currently, the test methods for introducing a needle into tissue and measuring the deflection are insufficient for our purposes. Therefore, this thesis serves to create a better test apparatus for taking these measurements.

1.2 Current Existing Experiments

A review of literature indicates current existing experimental setups give an incomplete picture of the interaction between tissue and needles in two ways. First, most only focus on initial puncture (until needle tip penetrates) - not deep puncture. In deep puncture, there are other effects, like friction, which need to be taken into account because they significantly affect the accuracy and maneuverability of the needle in tissue. Second, it does not study the full range of velocities (does not include velocities above 250 mm/s). At higher velocities, some properties of tissue change and there are potentially other phenomena acting on the needle that these prior tests have not adequately considered.

It is generally stated in the literature that faster motions of a sharp tool or needle cause less tissue deformation during cutting or penetration of a biological material due to its viscoelastic nature [3] but so far this has only been shown up to speeds of 250 mm/s. Experimental setups, such as the one featured in Figure 3, combine a linear stepper motor and a force sensor to insert the needles at a constant speed into the test sample for this low range of speeds. In addition, in-vivo experiments have also been conducted that substantiate this claim. [3]
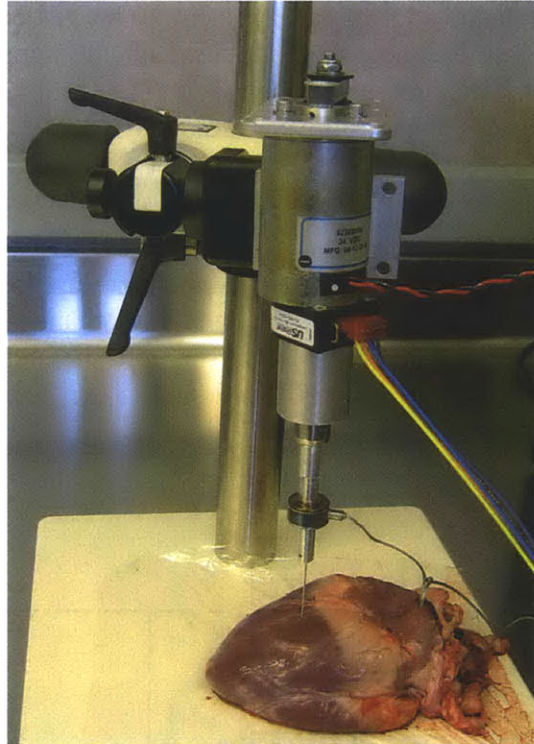
Figure 3: Typical experimental setup featuring sample, linear actuator, needle, and force gauge.
[3]

The stepper motor limits the available speeds for testing. In order to fully capture the dependence of tissue deflection on insertion velocity, a test setup is needed to not only address these lower speeds but also speeds up to and including 5 m/s. 5 m/s is a practical limit for suggested devices that insert at higher velocities. This is based on calculations based on a proposed device. This device may use a compression spring to store and release energy. In this case the calculations were done for a spring of 1000 N/m, compressing an inch, and accelerating a body roughly 0.1 kg in mass. Using conservation of energy (spring to kinetic), the maximum velocity this system can achieve is 8 m/s given no other losses. For this reason, 5 m/s is a good limit for this testing because it is a conservative estimate on the speed one could achieve. Tests, such as this one, also do not directly measure tissue deflection throughout the entire experiment but instead, run tests to find rupture deflection constants as well as relaxation constants such that the deflection can be calculated from the measured force. In developing a more universal experimental setup an improved method of tracking tissue deformation throughout the considered penetration must be determined.

2. Vertical Test Apparatus

2.1 Description of Test Apparatus

The first test setup concept involves a variation on a drop test experimental setup. It contains a guide rails for moving a needle into a sample at the end of travel. The needle travels on a moving component hereafter referred to as the dropping carriage.

In this setup, the dropping carriage with a needle attached using a luer lock is released into a sample of ex-vivo animal tissue. The dropping carriage will be stopped such that the needle

9

penetrates the tissue to a depth of approximately 3 cm. The velocity of the dropping carriage will be measured using a Vernier Photogate™ placed on the support structure in the region interest, in other words, in the region of impact. The dropping carriage provides two interferences for the Photogate™, which allows a pulse time to be measured between when the first section of the dropping carriage falls, and stops when the second section falls through the Photogate™. The collection rate should be set at 10000 samples/second to get the most precise measurements of velocity possible.

The needles are marked with laser markings 0.5 mm apart up the length of the shaft. During impact, high-speed video will be obtained of the sample at a camera angle oblique to the tissue surface plane. The moment the needle enters the tissue until the end of impact will be recorded. Figure 4 shows how the relevant deflection of the tissue will be calculated from the measurable quantities in the video.
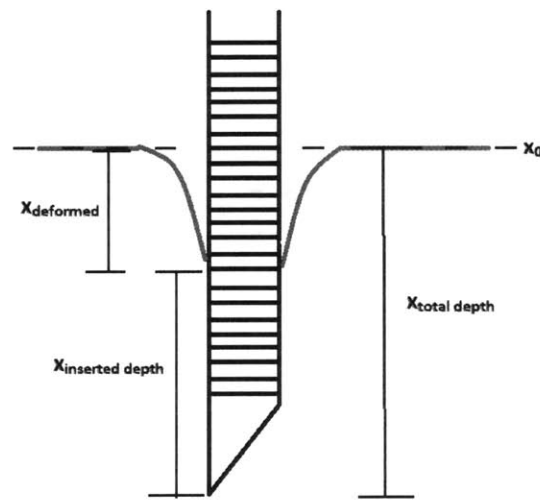
Figure 4: Needle depth diagram with tissue and needle featuring 0.5 mm laser markings. $x_{deformed}$ is shown, the quantity of interest.

The deformation will be calculated using Equation 1.

$$x_{deformed} = x_{total\ depth} - x_{inserted\ depth} \tag{1}$$

$x_{inserted\ depth}$ will be measured by taking the zero when the needle shaft first enters the tissue and measured by how many laser marks have entered the tissue. This measurement has a precision of 0.5 mm. Fiber optic strands of 0.5mm in diameter will be threaded through the needles and illuminated with laser light. These strands will provide a better visual reference on the video recording for when the tissue has been transferred from the bevel to the shaft of the needle. The inserted depth will be acquired via high-speed video of the setup during the impact, as shown in Figure 5. $x_{total\ depth}$ will be measured using a position sensor that can be correlated with the video footage to determine x_0 and then the total depth measured off of this. The camera

is placed such that it is at an angle oblique to the tissue, so that it can capture the entire puncture and deflection of tissue during insertion.
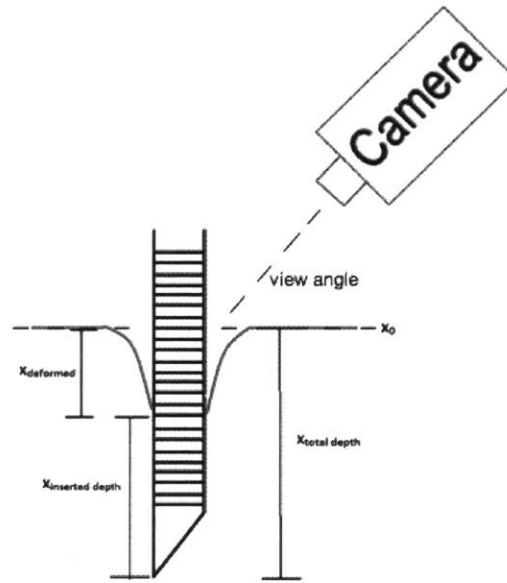
Figure 5: Schematic of test setup. Note this is not to scale. It shows the desired angle between the tissue deflection and the camera.

The first test apparatus achieves higher speeds than existing experiments by leveraging gravity in the form of a vertical drop test. To achieve the variety of speeds the dropping carriage will be released from different heights. The final velocity as a function of the height is shown in Equation 2.

$$v = \sqrt{2gh} \tag{2}$$

Where v is the final velocity, g is the acceleration due to gravity, and h is the height from which it is dropped. Due to the effects of gravity, the acceleration in the impact zone must be considered. Based on simple calculations the velocity does not appreciably increase in the impact zone at the higher speeds. However, at lower speeds this acceleration in the impact zone becomes more significant and therefore will be an area for improvement in the next iteration. These values are shown in Table 1.

Table 1: Effect of acceleration during travel in impact zone at various speeds.

Velocity At Impact (in m/s)	Final Velocity at End of Travel (in m/s)	Percentage of Total Velocity
1	1.26	26.0%
2	2.14	7.1%
3	3.10	3.2%
4	4.07	1.8%
5	5.06	1.2%

Also, due to the low magnitude of the resistance force as the needle punctures tissue the dropping carriage will not decelerate appreciably for this reason. This was found by comparing the force the dropping carriage exerts on the tissue and the typical measured forces form prior experiments. Equation 3 shows the force balance performed.

$$F_{net} = F_{carriage} - F_{tissue} \tag{3}$$

$F_{carriage}$ is the force exerted by the carriage, which is the mass of the carriage (0.5 kg) multiplied by the acceleration due to gravity. F_{tissue} is found using the upper limits of expected forces taken from the experiments conducted by Dupont, et al. [3] (0.6 N is the upper limit at the higher speeds). Therefore, the net force is approximately 4.3 N which is 87% of the original force from the carriage (4.9 N). It has not changed appreciably so therefore we may assume it will not decelerate appreciably.

2.2 CAD Model
Figure 6 shows a three-dimensional model of the vertical test apparatus.
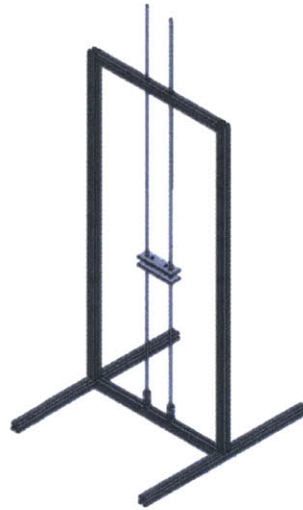
Figure 6: Three-dimensional model of vertical test apparatus.

This model shows the test apparatus structure featuring the support structure, guide rails, and dropping carriage. In the following figures, the features of this apparatus will be described.

Figure 7: Dropping carriage in the vertical test apparatus.

Figure 7 depicts the dropping carriage. Two ¼" shafts are used as guide rails to prevent the carriage from jamming due to moments on the bushings and slowing its fall. The white bushings shown are made of PTFE to minimize the amount of friction as the carriage falls along the rails. There are only three featured in this design because the fourth in the last hole causes the system to be over constrained so the hole will be drilled but left empty.

The dropping carriage is also set up as a system of two connected plates separated by 3 to 5 times the diameter of the rod based on Saint Venant's principal. [4] This is to further constrain the system to allow it to move more smoothly and to resist moments applied to the dropping carriage. The two plates are connected using two female threaded standoffs and shoulder screws. This connection method allows the plates to be attached to each other such that they are parallel.

Not shown here is the attachment method for the needle or the Bar Tape for the Vernier Photogate ™ sensor. The center of the bottom plate would be fit with a ¼-28 tapped hole in which a nylon male luer lock coupling would be attached to which any needle with a female luer lock end could be connected. The Bar Tape is attached to the right side of the dropping carriage where it would pass through the Photogate ™ to be attached to the support structure.

Figure 8: Top guide rail attachment to support structure.

Figure 8 shows the guide rails as they are attached to the aluminum inch T-slotted framing system. The guide rails are threaded so that the hex nuts shown can be tighted and the rods tensioned to improve the travel of the dropping carriage.
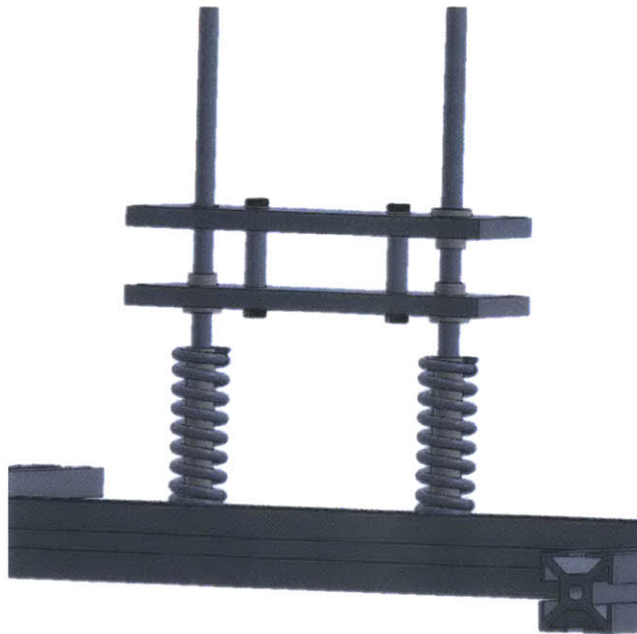
Figure 9: Dropping carriage shown in final dropped position.

Figure 9 shows the dropping carriage in the final position. The springs featured at the end of the guide rails are used to bring the carriage to a stop in less than 0.3". These springs are

also a chosen length to allow an adequate tissue sample to be placed in this area such that when the needle has penetrated to full depth the tip does not experience edge effects. Bushings keep the springs aligned with the guide rails. Finally, the guide rails are attached to the aluminum inch T-slotted framing system with special T-slot nuts into which the end of the rod can be screwed in to.

2.3 Building the Apparatus

Table 2: Bill of materials for the vertical test apparatus.

Item Number	Description	Quantity
1	Aluminum Inch T-Sloted Framing System	16 ft.
2	90 Degree Bracket, 4 Hole for T-Slotted Framing System	8
3	¼" Precision Ceramic-Coated Aluminum Shaft, 48"	2
4	PTFE Flanged Sleeve Bearing for ¼" Shaft Diameter	3
5	T-Slotted Framing System End-Feed Fastener	30
6	¼-20 Steel Hex Nuts	2
7	Steel Compression Spring	2
8	White Delrin Acetyl Resin Tube	4 in
9	Stainless Steel Female Threaded Standoff	2
10	Stainless Steel Shoulder Screw	4
11	¼ in Thickness Aluminum Sheet	1 ft^2
12	Plastic Male Luer Lock Coupling	1

Table 2 features the bill of materials used in the construction of the test apparatus shown in the figures below.

Figure 10: Dropping carriage without needle sample. Shoulder bolts, PTFE bushings, and sliding rods are shown.
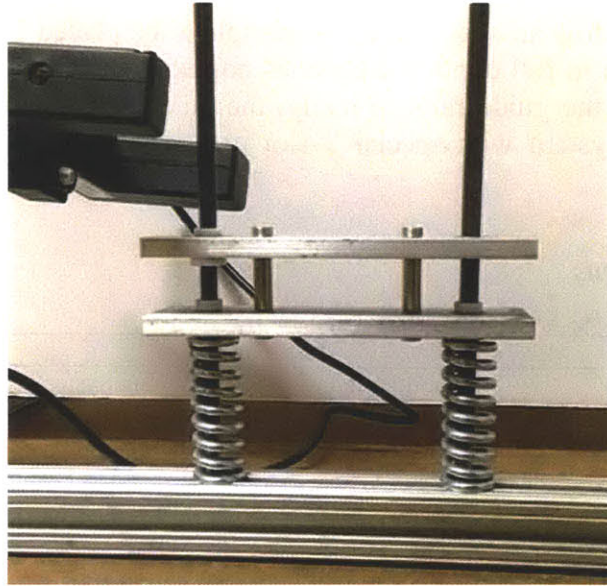
Figure 11: Dropping carriage shown at the bottom of travel. Photogate sensor mounted to measure speed of dropping carriage as it falls. Springs shown to bring dropping carriage to a full stop.

Figure 10 and Figure 11 show the actual construction of the test apparatus and feature the highlighted sections shown before in the three-dimensional model as well as the included Photogate ™ sensor.

2.4 Areas for Improvement

The construction of the vertical test apparatus revealed several areas for improvement. As previously mentioned, at lower speeds the acceleration in the impact zone is a larger percentage of the overall desired velocity. In the next iteration, this will be addressed and a method developed to minimize the effects of gravity at lower speeds.

In addition, the dropping carriage has a significant amount of friction as it slides along the guide rails which prevent it from reaching the desired 5 m/s even if released from its maximum possible height. Sample tests were run using the Photogate™ sensor to measure the speed of the dropping carriage in the region of impact. In these tests speeds of $3.53 \pm 0.09 \frac{m}{s}$ were achieved. This is far from the desired 5 m/s due largely to the high levels of friction. In the next iteration, a different bushing should be used such as an air bushing so that the friction will be negligible. The variability of final velocities could also be reduced by creating a more precise release mechanism. In this case, the dropping carriage was released by hand from the highest point possible, however, in the next iteration an electromagnet releasing it from the same height each time could help reduce this variation. The dropping carriage was over-constrained in this iteration because it had four separate points fixing it to the guiding rails. During assembly, it was difficult to get all four holes to align on the two guide railings after the plates had been fixed using the shoulder screws. Therefore, to alleviate this, the last PTFE bearing was omitted and instead, three holes with bushings were used to align the dropping carriage to the rails. The next

16

iteration will only have three fixed points through which a carriage will fall in order to prevent over-constraint but also provide enough stability so that the dropping carriage falls smoothly.

3. Inclined Plane Test Apparatus

3.1 Description of Test Apparatus

The inclined plane test apparatus is similar in concept to the vertical test apparatus but improves on several areas. As mentioned before, the acceleration due to gravity for the lower speeds is a larger proportion of the desired speed so the inclined plane concept is used to reduce the effects of gravity. Figure 12 gives an overview of the concept.
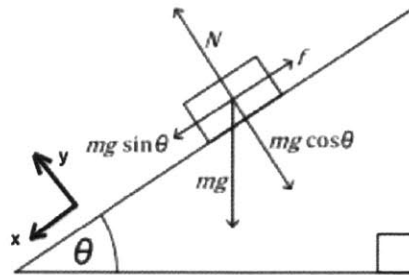
Figure 12: Free body diagram of inclined plane and relevant forces [1].

In this case the relevant force carrying the dropping cage down the inclined plane is described by Equation 4.

$$F_x = m \, g \sin \theta - f \tag{4}$$

Where m is the mass of the object falling, g is the acceleration due to gravity, θ is the angle of the inclined plane to the horizontal and f is the force due to friction. Since this apparatus will run on air bearings, the friction is negligible and can be ignored. Equation 4 demonstrates how at smaller angles, the sine term approaches zero thus reducing the total force and therefore reducing the effects of gravity when the carriage is released on a plane at a low angle to the horizontal. Equation 5 shows the relationship of the test apparatus angle on the final velocity assuming the carriage is released from rest.

$$v_{final} = \sqrt{v_i^2 + 2g * \sin \theta * d} \tag{5}$$

Where d is the distance traveled (in this case 3 cm in the impact zone), v_{final} is the final velocity and v_i the velocity at impact.

Assuming a total travel length of 1.5 m (the travel length that allows a final velocity of 5 m/s when released from vertical), Table 3 shows the comparison between velocity at impact versus velocity at stop and the total impact of the acceleration due to gravity in this region.

Table 3: Effect of acceleration during travel in impact zone at various speeds on an inclined plane.

Velocity At Impact (in m/s)	Final Velocity at End of Travel (in m/s)	Angle of Inclined Plane (in degrees)	Percentage of Total Velocity
1	1.03	5	2.5%
2	2.03	10	1.3%

3	3.03	15	0.8%
4	4.05	45	1.3%
5	5.06	90	1.2%

Velocity precision up to 0.1 m/s is desired. Based on Equations 4 and 5, the only changing parameter is that of the inclined plane since the carriage will be released at the same point each time. Therefore, the only way to get this precision in the velocity is to control the angle. Therefore, the angle of the table will be measured using a digital angle gauge precise to 0.1°. The table will also feature a worm gear system to allow the entire table to be cranked to a precise angle and fixed during the test.

As previously mentioned, this apparatus will leverage the frictionless quality of air bushings. Different from the previous apparatus instead of a small dropping carriage, three air bushings will be used to guide two rails that will fall. In this case, the motion occurs in the rails and not a carriage. The same Vernier Photogate ™ will be used to measure the velocity.

The following section will describe in further detail the implementation of these improvements alongside images of a three-dimensional model.

3.2 CAD Model

Figure 13 to Figure 18 are images of three-dimensional model of the inclined plane test apparatus in an isometric view.
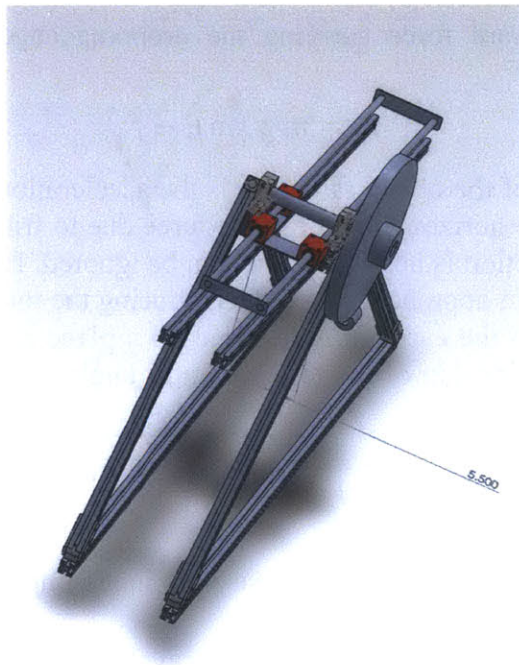
Figure 13: Inclined plane test apparatus in isometric view.

The support structure is triangular to provide support as the heavy rods fall through the air bushings. In later figures, attention will be drawn to the smaller features not shown here.

18
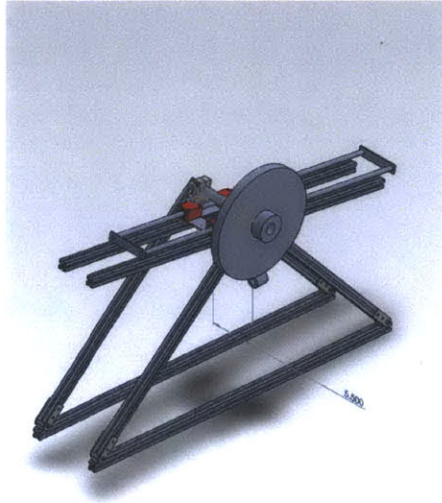
Figure 14: Inclined plane test apparatus shown in another isometric view.

Although not shown here, the large round wheel is a gear and the cylinder below it the worm. These are simple representations of the worm and gear drive that will be used to tilt the table to the desired angle and hold it in place during the test. The gear shaft is attached to the aluminum T-slotted framing pieces that support the red air bushings so that the tilting plate can be tilted then fixed. Figure 15 shows a close-up of the shaft and gear system.
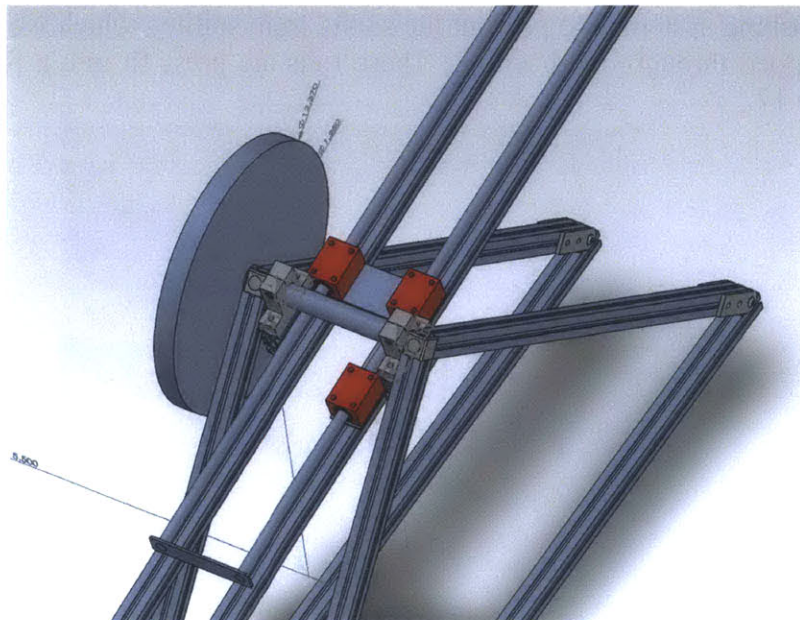
Figure 15: Close up of shaft and gear system.

As shown here, the shaft is held in place by two brackets attached to smaller T-slotted frame pieces. The shaft is then run out to the side where the gear is located.

Figure 16 shows a close up image of the air bushing system.
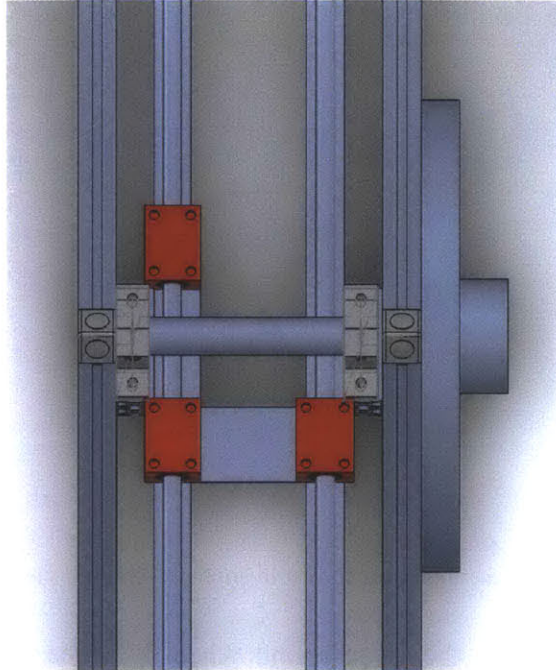
Figure 16: Air bushing system.

As shown in Figure 16, three air bushings are attached to an L-shaped plate. One stainles steel rod runs through the left two bushings and one runs through the right bushings. The two rod and three bushing system is to prevent the shafts from spilling which would occur if one rod was simply dropped through one bearing. These rods are press fit into a fixing plate which is shown in Figure 17.
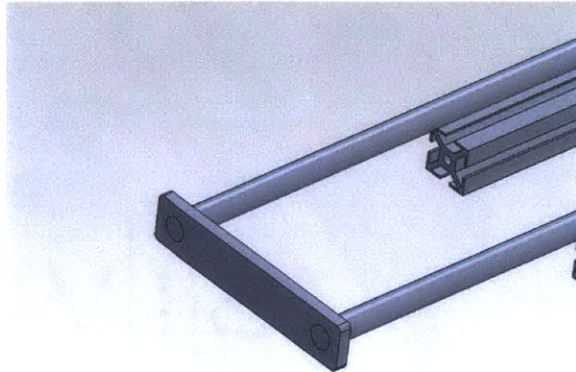
Figure 17: Close up image of fixing plate.

The fixing plate, is used to keep the rods parralel and traveling together during the test. Figure 18 shows a close up of the L-shaped plate. This part is critical as it aligns the air bearings such that they stay parallel.
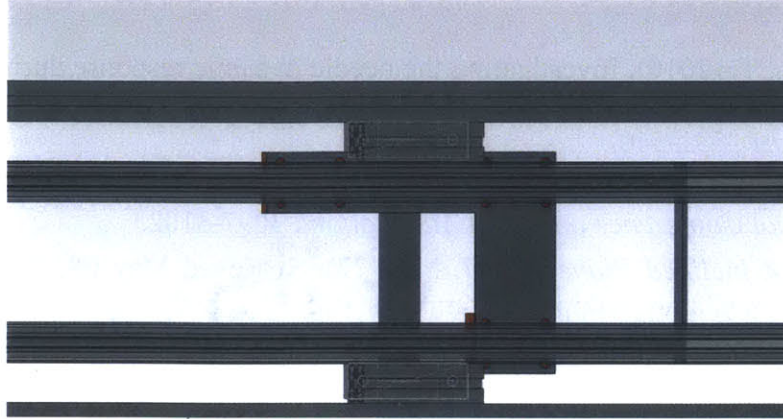
Figure 18: Close up image of L-shaped plate.

The L-shaped plate features twelve holes used to fix the air bushings into place. These are clearance holes such that the first two air bearings can be tightened down, the rods attached to the end fixing plates, and then the other air bearing tightened so that the parallel alignment is maintained. They will be fixed down using two washers with grease and a nut placed such that the two washers are separated by grease and the nut placed on the bottom to tighten them into place against a bolt that runs from the air-bushing block through the plate. This way, the rotation of the bolts as they are tightened does not cause the whole system to move and become misaligned.

4. Conclusions

This thesis consisted of designing and building a test apparatus to be able to experimentally investigate a proposed dynamic model for tissue. To this end a first round vertical test apparatus was designed, modeled, and built. After building it was evaluated for its performance and suggestions for improvement were made. These suggestions included switching the bearings to reduce friction as the dropping carriage falls, an electromagnet dropping carriage release mechanism, and making the apparatus an inclined plane as a way to reduce the effects of gravity at lower desired speeds. These improvements were included in a second model for an inclined plane test apparatus. Overall, both of the designs could be used to collect data to experimentally verify this proposed dynamic tissue model as well as serve as a model for other potential tissue deflection experiments. In the future, the inclined plane test apparatus would be assembled and evaluated for its performance as far as achieving desired speed, ability to collect deflection data on a tissue sample, and repeatability of such experiments. To expand upon the work done to design the test apparatus a more cohesive and explicit test method should be developed such that further tests could be run with consistency.

Bibliography

[1] Aljaafreh, T. (2010). Investigating the needle dynamic response during insertion into soft tissue. *Proceedings of the Institution of Mechanical Engineers Part H - Journal of Engineering in Medicine Report* , 531-540.

Dupont, P. a. (2009). Fast Needle Insertion to Minimize Tissue Deformation and Damage. *IEEE International Conference on Robot Automation* , 3097-3102.

Free Body of Inclined Plane. (2007, May 27). Retrieved May 08, 2013, from Wikipedia: http://upload.wikimedia.org/wikipedia/commons/8/85/Free_body.svg

Slocum, A. (2008, February 01). *FUNdaMENTALS of Design*. Retrieved May 08, 2013, from MIT Precision Engineering Research Group: pergatory.mit.edu/resources/FUNdaMENTALS.html